BIOCHEMISTRY
including biophysical chemistry & molecular biology

Article

pubs.acs.org/biochemistry

Role of Propionates in Substrate Binding to Heme Oxygenase from *Neisseria meningitidis*: A Nuclear Magnetic Resonance Study

Dungeng Peng,[†] Li-Hua Ma,[†] Kevin M. Smith,[†] Xuhong Zhang,[‡] Michihiko Sato,[§] and Gerd N. La Mar*[,†]

[†]Department of Chemistry, University of California, Davis, California 95616, United States

[‡]Department of Biochemistry and Molecular Biology, Yamagata University Graduate School of Medical Science, Yamagata 990-9585, Japan

[§]Central Laboratory for Research and Education, Yamagata University Faculty of Medicine, Yamagata 990-9585, Japan

Supporting Information

ABSTRACT: Heme oxygenase (HO) cleaves hemin into biliverdin, iron, and CO. For mammalian HOs, both native hemin propionates are required for substrate binding and activity. The HO from the pathogenic bacterium *Neisseria meningitidis* (*Nm*HO) possesses a crystallographically undetected C-terminal fragment that by solution ^{1}H nuclear magnetic resonance (NMR) is found to fold and interact with the active site. One of the substrate propionates has been proposed to form a salt bridge to the C-terminus rather than to the conventional buried cationic side chain in other HOs. Moreover, the C-terminal dipeptide Arg208His209 cleaves spontaneously over ∼24 h at a rate dependent on substituent size. Two-dimensional ^{1}H NMR of *Nm*HO azide complexes with hemins with selectively deleted or rearranged propionates shows that all bind to *Nm*HO with a structurally conserved active site as reflected in optical spectra and NMR nuclear Overhauser effect spectroscopy cross-peak and hyperfine shift patterns. In contrast to mammalian HOs, *Nm*HO requires only a single propionate interacting with the buried terminus of Lys16 to exhibit full activity and tolerates the existence of a propionate at the exposed 8-position. The structure of the C-terminus is qualitatively retained upon deletion of the 7-propionate, but a dramatic change in the 7-propionate carboxylate ^{13}C chemical shift upon C-terminal cleavage confirms its role in the interaction with the C-terminus. The stronger hydrophobic contacts between pyrroles A and B with *Nm*HO contribute more substantially to the substrate binding free energy than in mammalian HOs, "liberating" one propionate to stabilize the C-terminus. The functional implications of the C-terminus in product release are discussed.

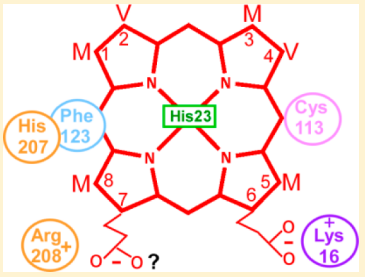

Heme oxygenase (HO) is the widely distributed enzyme[1] that utilizes hemin as both a substrate and a cofactor to stereospecifically cleave a single meso position to generate biliverdin, iron, and CO, proceeding via the intermediates depicted in Scheme 1. In mammals, the three products serve as a precursor to the powerful antioxidant bilirubin, as a source of 97% of the required iron, and as a neural messenger, respectively.[2−6] In plants and photosynthetic bacteria, the product open tetrapyrrole serves as a precursor to light-harvesting pigments,[7] while the released iron is vital to infection for some pathogenic bacteria.[2,4] The mammalian HOs have been the most extensively studied,[3] and in spite of only limited sequence homology,[4] both the characteristic α-helical topology[8−13] and the mechanism[2,4,6] are conserved among other HOs. The relatively loose binding of substrate by HOs, as evidenced by both numerous vacancies and the variable position of structural elements,[8−13] involves an axial bond to a His, two salt bridges between the ubiquitous propionates, and two suitably positioned cationic side chains as depicted in Figure 1A; the remaining interactions are relatively weak van der Waals contacts with pyrroles A and B.

The stereoselectivity of the cleavage arises from the steric effect of the distal helix that tilts the active Fe^{3+}-OOH toward one meso position while blocking the three remaining meso positions.[9−13] The particular meso position cleaved depends on the in-plane orientation of the substrate relative to the distal helix. Only the α-meso position is cleaved in mammalian HOs. The crucial role of propionate links in determining the in-plane orientation, and hence stereoselectivity, of substrate cleavage is confirmed by studies of human HO (hHO)[14] mutants in which repositioning the cationic side chains leads to an ∼90° in-plane rotation of the substrate with concomitant conversion of α-meso to mixed β,δ-meso cleavage. Earlier studies of hHO, with a variety of modified substrates,[15,16] have revealed that while a wide range of substituents on pyrroles A and B is tolerated (Figure 1B), the two propionates at positions 6 and 7 must both be conserved to retain activity.

In spite of sharing the same folding topology and mechanism with mammalian HOs, the HOs from pathogenic bacteria[2,4−6] exhibit some distinct properties relative to function. Three pathogenic bacterial HOs have been structurally characterized, those from *Neisseria meningitidis*[9,11] (*Nm*HO), *Pseudomonas aeruginosa*[13] (*Pa*HO), and *Corynbacterium diphtheria*[12] (*Cd*HO). *Cd*HO, which is the most homologous[4,6,12] to

Received: June 12, 2012
Revised: August 21, 2012
Published: August 22, 2012

Scheme 1

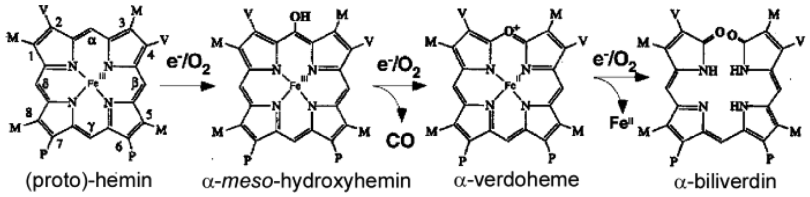

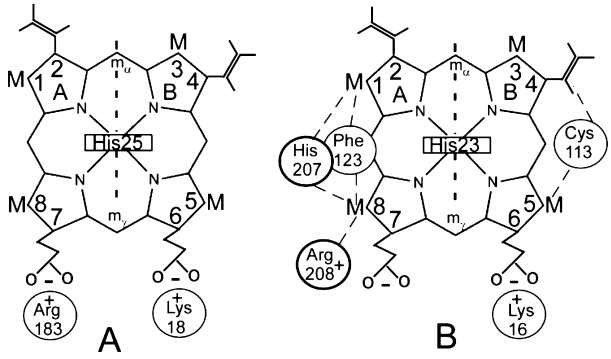

Figure 1. Orientation of native protohemin IX within the active site of (A) human HO[8] (hHO) showing the key salt bridges of the 6-propionate with the side chain of Lys18 and the 7-propionate with the side chain of Arg183 and (B) *Nm*HO[9,11] showing the conserved salt bridge between the 6-propionate and Lys16, as well as two residues, Cys113 and Phe123, that are key to the determination of the orientation of the substrate in the active site. The contacts of two residues not detected in the crystal structure, His207 with M_1 and M_8 and Arg208 with M_8, are also shown in bold.

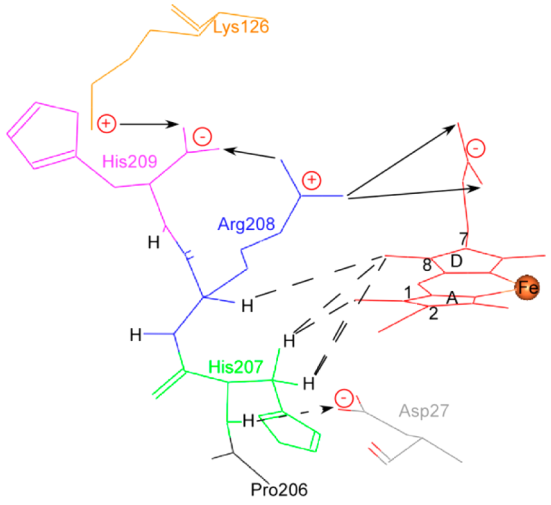

Figure 2. Proposed molecular model[24] for the C-terminus of substrate-bound *Nm*HO determined by limited energy minimization based on the proposed donor–acceptor interactions (arrows). His207 (green) peptide NH H-bond donor to carboxylate of Asp27 (gray) and the Arg208 (blue) guanidyl group salt bridges to the carboxylates of the 7-propionate (red) and C-terminal His209 carboxylate, which in turn is an acceptor for the side chains of both Lys126 and Arg208.

mammalian HOs in sequence and structure, exhibits the same stereoselectivity and sensitivity to mutation,[17] a similar 90° in-plane rotation, and altered stereoselectivity, upon mutation of cationic residues,[18] compared to those of mammalian HOs.[14,19] *Pa*HO exhibits[13,20] mixed *β*,*δ*-meso cleavage due to an ∼90° in-plane rotation of protohemin IX relative to that in mammalian HOs, resulting from the rearrangement of cationic side chains in the wild-type protein.

*Nm*HO exhibits numerous distinct properties. While there is normal *α*-meso cleavage consistent with protohemin IX oriented as depicted in Figure 1B, the structure of the active site is more compact and has fewer vacancies[9,11] than in other HOs. The roles of the propionates in the crystal structures are not well-defined, and key C-terminal residues are undetected.[9,11] In contrast, solution nuclear magnetic resonance (NMR) has demonstrated that the C-terminal fragment, His207Arg208His209, is, in fact, ordered and interacts with the active site.[21−24] A molecular model based on limited energy minimization and using as constraints limited NOESY data and a series of proposed salt bridges suggested by the crystal structure has been offered[22,24] and is reproduced in Figure 2. We note that this model utilizes one of the two propionates (at native PH*IX* position 7 in the crystal[9,11]), leaving but one propionate to make the conventional salt bridge to the protein matrix. Surprisingly, the C-terminus of *Nm*HO cleaves spontaneously upon substrate binding[22] to yield a complex with an increased rate of product release. The fact that the necessary acceleration of product release[25] in mammalian HOs occurs[3] by the binding of biliverdin reductase (BVR) at the exposed substrate site[26] that is homologous to the site of the C-terminal interaction in *Nm*HO demands a more quantitative understanding of the C-terminus in the latter complex.

We have pursued detailed ^{1}H NMR studies[21−24,27] of systematically perturbed interactions of the substrate with *Nm*HO in general, and its C-terminal fragment in particular, to evaluate the molecular model (Figure 2) and ascertain the structural features that favor the facile cleavage of the C-terminus. Studies of the three sequential C-terminal deletion mutants directly confirmed[24] the substrate contacts to His207 and Arg208 and indicated the existence of a salt bridge for the C-terminal carboxylate with a cationic side chain of both Arg208 and Lys126. Systematic variation of substrate pyrrole A and B substituents revealed[27] a much tighter interaction between the substrate and protein matrix, and hence much stronger descrimination between the alternate substrate orientation about the *α*,*γ*-meso axis, than in any other HO[20,28−30] and revealed that the C-terminal cleavage rate increased[24] as the size of the pyrrole A substituent decreased. Herein, we complete these studies by perturbing the substrate propionates, both by replacement of individual propionates with methyls and by interchanging methyl and propionate on one pyrrole, to ascertain whether the propionates must be conserved for activity, as found in mammalian HOs,[15,16] and identify the interactions of the propionates at each position.

To this end, we take advantage of a series of modified hemins[31,32] depicted in Figure 3 designed to illuminate the interaction of substrates with *Nm*HO relative to that in mammalian HOs; labeling of these substrates is based on modifications of protohemin-IX (PH*IX*) and 2,4-dimethyldeuterohemin-IX (DMDH*IX*). We emphasize the low-spin azide complex in which the novel orbital ground state[33] results in

dx.doi.org/10.1021/bi3007803 | *Biochemistry* 2012, 51, 7054−7063

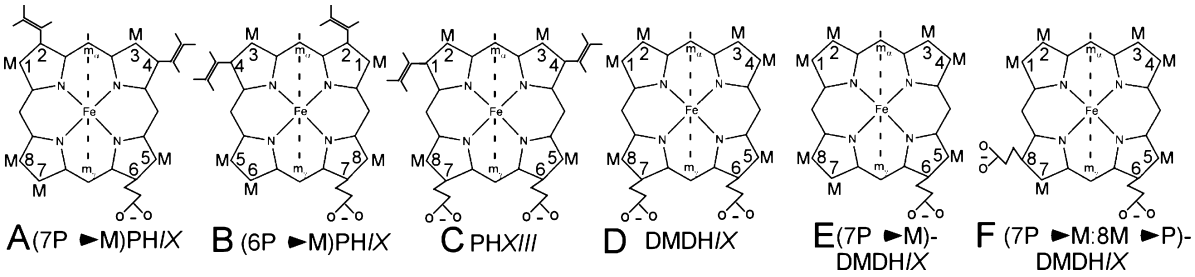

Figure 3. Structure and labeling of modified hemins relevant to this study (M = methyl). The orientation of the vinyl groups relative to the adjacent methyl on the same pyrrole is shown as deduced by NOESY cross-peaks in solution: (A) 7-depropionate-, 7-methyl-protohemin-IX [(7P→M)PH*IX*], (B) 6-depropionate-, 6-methyl-protohemin-IX [(6P→M)PH*IX*], (C) protohemin-XIII (PH*XIII*), (D) 2,4-dimethyldeuterohemin-IX (DMDH*IX*), (E) 7-depropionate-, 7-methyl-2,4-dimethyldeuterohemin-IX [(7P→M)DMDH*IX*], and (F) 7-depropionate-7-methyl, 8-demethyl-8-propionate-2,4-dimethyldeuterohemin-IX [(7P→M:8M→P)DMDH*IX*]. The orientations of the substrates, relative to the protein matrix, are depicted as found in the active site shown in Figure 1B, and the determined vinyl orientations are shown at *cis* (vinyl H_β next to methyl on the same pyrrole) or *trans* (vinyl H_α next to methyl on the same pyrrole). The arbitrary labeling of the pyrrole positions in 2-fold symmetric PH*XIII* and in the DMDH*IX* derivatives corresponds to the same numbered position of PH*IX* in the crystal structure.

strongly contact-shifted, and hence resolved, signals[24,27,34,35] for the protons on the substrate edge exposed to solvent that makes contact with the C-terminus (see Figure 2). While relaxation for the azide complexes is somewhat stronger for the more frequently studied cyanide complexes,[36] it does not seriously interfere with effective two-dimensional (2D) NMR analysis,[24,27,35] and the physiological oxy complex is more reasonably modeled by the bent azide than the linear cyanide ligand.

■ MATERIALS AND METHODS

Materials. The wild-type (WT) *N. meningitidis* heme oxygenase (*Nm*HO) was prepared and purified as described in detail previously.[21] The two derivatives of protohemin-IX with selective methyl for propionate substitutions, 6-depropionate-, 6-methyl-protohemin-IX [(6P→M)PH*IX*] and 7-depropionate-, 7-methyl-protohemin-IX [(7P→M)PH*IX*], 2,4-dimethyldeuteroheme-IX (DMDH*IX*), and protohemin-XIII (PH*XIII*) (which possesses the symmetric 1,4-divinyl arrangement) are the same as described in detail previously.[32] The two hemins with selective removal or rearrangement of propionates, based on 2,4-dimethyldeuterohemin-IX (DMDH*IX*), are 7-depropionate-, 7-methyl-2,4-dimethyldeuterohemin-IX [(7P→M)DMDH*IX*] and 7-depropionate-7-methyl-, 8-demethyl-8-propionate-2,4-dimethyldeuterohemin-IX [(7P→M:8M→P)-DMDH*IX*], which were prepared as described previously.[31] The positions on the DMDH*IX* and PH*XIII* derivatives are labeled (see Figure 3) on the basis of the orientation of native protohemin-IX in the crystal structure, as shown in Figure 1B.[9,11] The carboxylates of native protohemin-IX were ∼90% singly or doubly labeled with ^{13}C to yield 6-($^{13}C_\gamma O_2^-$)PH*IX* and 6,7-($^{13}C_\gamma O_2^-$)$_2$PH*IX*, respectively, as described previously.[37]

The 1:1 complexes of the substrate of interest with *Nm*HO were prepared as described previously[21] for the PH*IX* and DMDH*IX* complexes, except that the monopropionate hemins were dissolved in 95% H_2O and 5% pyridine, with the pyridine removed immediately after preparation via Sephadex column chromatography, as described previously for the reaction with globins.[38] The quantitative incorporation of each substrate into *Nm*HO was confirmed both by the characteristic UV−visible spectra as the cyanide complexes and by the identification of the signals in the ^1H NMR spectrum as the azide complexes. Samples for ^1H NMR were concentrated by ultrafiltration to yield ∼2 mM samples in 50 mM phosphate and 75 mM azide (pH ∼7.1).

UV−Visible Spectroscopy. Spectra were recorded on a Varian Cary 50 UV−visible spectrometer over the range of 200−800 nm at a rate of 50 nm/s; 32 transients were averaged. The sample *Nm*HO substrate complexes were 30 mM in cyanide and 50 mM in phosphate (pH 7.1).

In Vitro Enzyme Assay. The activity of the various substrate complexes of *Nm*HO was determined by following by UV−visible spectroscopy the effect of the reaction with ascorbate, in the presence of the iron chelator desferrioxamine, in the conversion of hemin to biliverdin, as described in detail previously.[21] Subsequently, the product biliverdin was reacted with rat biliverdin reductase, prepared as described previously,[39] and NADPH to generate bilirubin.

NMR Spectroscopy. ^1H NMR data were collected on Bruker AVANCE 500 and 600 spectrometers operating at 500 and 600 MHz, respectively. ^1H chemical shifts are referenced to 2,2-dimethyl-2-silapentane-5-sulfonate (DSS) through the water resonance calibrated at each temperature. Reference spectra were collected over a 65 ppm spectral width and a repetition rate of 2.5 s^{-1}; 600 MHz NOESY spectra[40] (mixing time of 40 ms, repetition rate of 1.5−2.5 s^{-1}) and 500 MHz Clean-TOCSY spectra[41] (to suppress the ROESY response; 25°, 35 °C, spin lock of 25 ms; repetition rate of 1−2 s^{-1}) were recorded over a bandwidth of 20 and 45 ppm (NOESY) and 20 ppm (TOCSY) using 512 t_1 blocks of 128 and 256 scans each consisting of 2048 t_2 points. 2D data sets were apodized by 30° or 45° sine-squared bell functions and zero-filled to 2048 × 2048 data points prior to Fourier transformation.

^1H-decoupled ^{13}C NMR spectra were recorded at 125 MHz on a Bruker AVANCE 500 spectrometer over a bandwidth of 300 ppm at a repetition rate of 1 s^{-1} at 25 °C utilizing 32K data points. The ^{13}C chemical shifts were indirectly referenced to the proton spectrum.[42]

■ RESULTS

Structural Integrity of Propionate-Modified Substrate Complexes. The reaction of (6P→M)PH*IX* and (7P→M)PH*IX* with *Nm*HO in the presence of excess cyanide resulted in the same characteristic changes in their UV−visible spectra that were observed for native PH*IX*, while reaction of (7P→M)DMDH*IX* and (7P→M:8M→P)DMDH*IX* with *Nm*HO in the presence of excess cyanide resulted in the

dx.doi.org/10.1021/bi3007803 | *Biochemistry* 2012, 51, 7054−7063

same UV−visible spectral changes that were observed for the DMDH*IX* complex (Figure S1 of the Supporting Information). The near identity of the UV−visible spectra of the *Nm*HO complexes with those of the propionate-modified and "normal" dipropionate substrates supports the incorporation of the modified substrate into an environment that is essentially the same as that for PH*IX* and DMDH*IX*. The ^{1}H NMR spectra of the azide complexes of (7P→M)PH*IX* and (6P→M)PH*IX* are presented as spectra B and C of Figure 4, respectively, where

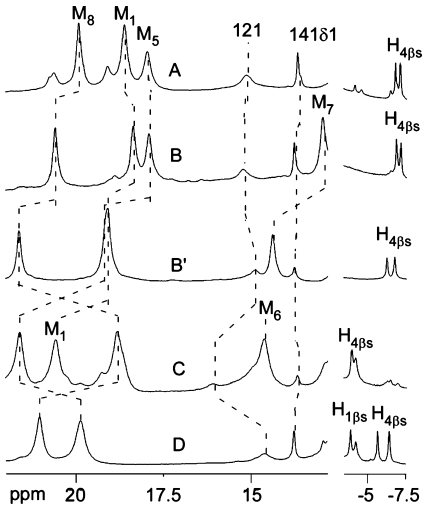

Figure 4. Resolved portions of the 600 MHz ^{1}H NMR reference spectra, in ^1H_2O, 50 mM phosphate, and 75 mM azide (pH 7.1) at 25 °C, of (A) WT *Nm*HO−PH*IX*-N_3, (B) WT *Nm*HO−(7P→M)PH*IX*-N_3, (C) WT *Nm*HO−(6P→M)PH*IX*-N_3, and (D) WT *Nm*HO−PH*XIII*-N_3 complexes. The spectrum for the aged or C-terminally cleaved *Nm*HO complex, *Nm*HO^X−(7P→M)PH*IX*-N_3, is shown as spectrum B′.

they can be compared with that of the complex with native PH*IX* (Figure 4A). Also included is the ^{1}H NMR spectrum of the azide complex for the 2-fold symmetric PH*XIII* (Figure 4D). The NMR spectra of the *Nm*HO azide complexes of (7P→M)DMDH*IX* and (7P→M:8M→P)DMDH*IX* are shown as spectra B and C of Figure 5, respectively, and can be compared with that of the previously characterized DMDH*IX* complex[24] shown in Figure 5A. The NMR spectra shown as spectra B−D of Figure 4 and spectra B and C of Figure 5 display a strongly dominant single set of hyperfine-shifted methyl signals that indicate a unique orientation of the modified substrates within an active site very similar to that observed for the normal dipropionate PH*IX* and DMDH*IX*.

Activity of Modified Substrate Complexes. The complexes with modified substrates all underwent reaction with ascorbate in the presence of the iron chelator, desferrioxamine, in a standard assay[22] that yielded UV−visible spectra with characteristic broad bands at ∼380 and ∼670 nm[43] indicative of biliverdin formation, with the resulting spectra largely indistinguishable from those of the related substrates with the two normal propionates (Figure S2 of the Supporting Information). Subsequent reaction of the biliverdin with rat biliverdin reductase[39] and NADPH afforded the spectra indicative of bilirubin formation. Thus, HO activity is conserved upon either deletion of one propionate or exchange between a propionate and methyl on the same pyrrole.

Substrate/Active Site Residue Assignment Protocols. Substrate protons for the major isomers in solution are labeled

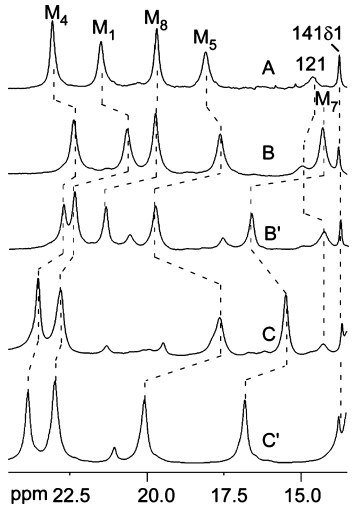

Figure 5. Resolved portions of the 600 MHz ^{1}H NMR reference spectra, in ^1H_2O, 50 mM phosphate, and 75 mM azide (pH 7.1) at 25 °C, of (A) WT *Nm*HO−DMDH*IX*-N_3, (B) WT *Nm*HO−(7P→M)DMDH*IX*-N_3, and (C) WT *Nm*HO−(7P→M:8M→P)DMDH*IX*-N_3 complexes. The NMR spectra of the "degraded" or C-terminally cleaved complexes, *Nm*HO^X−(7P→M)DMDH*IX*-N_3 and *Nm*HO^X−(7P→M:8M→P)DMDH*IX*-N_3, are shown as spectra B′ and C′, respectively.

$M_i(H_i)$ for the methyl (single proton) at pyrrole positions 1−8 (*i*) (see Figure 1). Residue protons are labeled by residue number and position; peptide protons are labeled by only position. Unambiguous assignment of the substrate resonances is obtained by characteristic NOESY connectivities about the periphery and is facilitated by the expected pattern of substrate hyperfine shifts.[24,27,35] On one hand, cross-peaks between a pair of methyls on the same pyrrole (adjacent to a common meso position) are strong (weak). Methyl−vinyl H_βs (H_αs) NOESY cross-peaks are strong for a vinyl oriented *cis* (*trans*) to its adjacent methyl[27] as depicted in Figure 3. On the other hand, the known orbital ground state for the azide complex places large π spin density[24,27,34,35] at only positions 1, 4, 5, and 8, such that methyl and vinyl H_αs appear strongly shifted to low field and the vinyl H_βs exhibit strongly upfield shifted and resolved resonances. Substrate chemical shifts for pyrrole α-substituents are listed in Table 1; complete substrate assignments and active site residue assignments are provided in Tables S1−S4 of the Supporting Information.

Active site residues are assigned sequence-specifically[44] by characteristic backbone NOESY cross-peaks among TOCSY-detected residues characteristic of an α-helix (data not shown) as described in detail previously for a series of *Nm*HO and hHO azide complexes.[24,27,35] These studies afford the assignments for the helical fragments: Thr19−Val26 (proximal helix) and Phe52−Lys54 and Tyr112−Gly116, Phe123−Phe125 (distal helix), Arg140−Leu142, and Ala180−Tyr184. The two residues central to establishing the orientation of a substrate in the active site[27] are Phe123 in contact with substituents at positions 1 and 8 and Cys113 in contact with substituents at positions 4 and 5 in the crystal structure (Figure 1B). Chemical shifts for the axial His23 are included in Table 1 and for other residues are provided in Tables S3 and S4 of the Supporting Information.

Seating of Propionate-Modified Substrates. To uniquely place modified substrates in the active site of *Nm*HO, we will describe the proton at a given position on

dx.doi.org/10.1021/bi3007803 | *Biochemistry* 2012, 51, 7054−7063

Table 1. Chemical Shifts for Variable Substrates[a] in Azide Complexes of WT *Nm*HO[b]

peak[e]	PH*IX*[c,d]	PH*IX*[d,e]	(6P→M)PH*IX*	(7P→M)PH*IX*	DMDH*IX*[c]	(7P→M)DMDH*IX*	(7P→M:8M→P)DMDH*IX*
$M_1(H_{1\alpha})$[f]	18.68	19.85	20.55	18.34	21.42	20.63	22.90
$M_2(H_{2\alpha})$	(10.32)	(10.22)	(10.75)	(9.04)	10.10	10.62	10.10
M_3	7.60	7.60	8.45	7.66	11.39	?	11.80
$M_4(H_{4\alpha})$	(11.78)	(18.60)	(18.65)	(11.82)	23.00	22.35	23.64
M_5	18.02	20.65	21.57	17.90	18.05	17.60	17.84
M_6	–		14.58	–	–	–	–
M_7	–		–	12.95	–	14.29	15.70
M_8	20.00	19.12	18.79	20.57	19.67	19.70	–
$H_{6\alpha1}$	9.62	–	–	9.78	8.73	8.38	9.90
$H_{6\alpha2}$	2.00	–		1.65	5.35	4.06	5.40
$H_{7\alpha1}$	9.82	10.13	9.38	–	12.17	–	–
$H_{7\alpha2}$	5.65	2.50	3.25	–	6.70	–	–
$H_{8\alpha1}$	–	–	–	–	–	–	13.81
$H_{8\alpha2}$	–	–	–	–	–	–	8.30
His23 $C_{\beta1}H$	12.56	12.67	12.74	12.65	12.65	12.85	12.77
His23 $C_{\beta2}H$	9.68	9.78	9.77	9.85	9.28	9.68	9.25

[a]Substrate structures and proton labels are shown in Figure 3. [b]Chemical shifts in parts per million, referenced to DSS, in ^1H_2O, 50 mM phosphate, and 75 mM azide (pH ~7.1) at 25 °C. [c]Crystallographic orientation, as in Figure 1B. [d]Orientation reversed about the α,γ-meso axis relative to that in the crystal (data taken from ref 24). [e]Orientation rotated 180° about the α,γ-meso axis relative to that in the crystal. [f]Vinyl H_α chemical shifts are given in parentheses; vinyl and propionate $C_\beta H$ chemical shifts are provided in Tables S1 and S2 of the Supporting Information.

the modified substrate, as labeled in Figure 3, and identify where each of those protons on the substrate is placed in the active site defined by the position of the PH*IX* proton in the crystal structure, as shown in Figure 1B.[9,11] Portions of the ^1H NMR NOESY spectrum of the *Nm*HO−(7P→M)PH*IX*-N_3 complex for assigning the substrate and active site residues relevant to substrate seating are shown in Figure 6. A weak cross-peak between two low-field methyls (Figure 6B) locates the M_1/M_8 pair, and an intense cross-peak of one of these to a more weakly low-field shifted methyl (Figure 6H) identifies the M_8/M_7 pair. Intense cross-peaks of high-field resolved vinyl H_βs

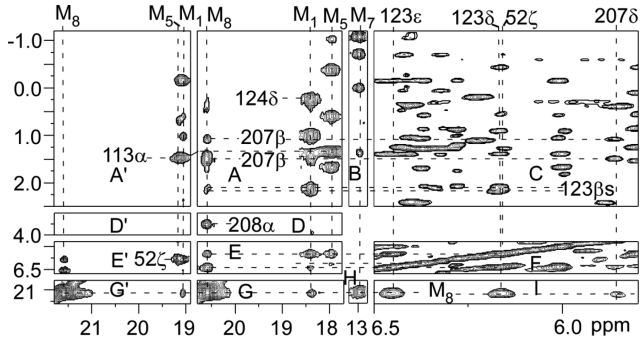

Figure 6. Resolved portions of the 600 MHz ^1H NMR NOESY spectrum, in ^1H_2O, 50 mM phosphate, and 75 mM azide (pH 7.1) at 25 °C, of the WT *Nm*HO−(7P→M)PH*IX*-N_3 complex, illustrating key intrasubstrate contacts (A, B, G, and H), substrate residue contacts (A, C−E, and I) for Phe52, Cys113, Phe123, Leu124, His207, and Arg208, and intraresidue contacts (C and F) for His207 that uniquely assign the substrate and determine the orientation of the substrate in the pocket. Noted are the His207 $C_\beta H$ and $C_\delta H$ contacts with M_8 (E and I) and His207 with M_1 (E). Panels A′, D′, E′, and G′ for the C-terminally cleaved *Nm*HO^X−(7P→M)PH*IX*-N_3 complex exhibit the same data as panels A, B, D, E, G, and H for the WT complex, except for the loss of the cross-peaks from His207 and Arg208 to M_8/M_1. All panels except C, F, and I utilize a 45 ppm bandwidth, a 2.5 s^{-1} repetition rate, and a 45° phase-shifted sine bell apodization; panels C, F, and I utilize a 20 ppm bandwidth, a 1.0 s^{-1} repetition rate, and a 30° phase-shifted sine bell apodization.

to a partially resolved methyl and a strongly low-field shifted H_α locate the 4-vinyl group and M_3 (not shown). The remaining low-field methyl exhibits cross-peaks to a moderately low-field shifted pair of H_αs and H_βs that identify the 5-methyl and 6-propionate. The M_1 cross-peaks to another vinyl H_βs locate the 2-vinyl group and establish that both vinyl groups are oriented *cis*, as in the crystal structure[9,11] for the PH*IX* complexes, as shown in Figure 3B. The M_1 and M_8 cross-peaks to Phe123 and the M_5 [and 4-vinyl (not shown)] cross-peak to Cys113 $C_\alpha H$ (Figure 6A) establish an orientation in which the lone propionate is in the position of the 6-propionate in the crystal structure (Figure 1B). M_1/M_8 contacts to two residues not predicted by the crystal structure are observed to both the ring $C_\delta H$ (Figure 6I) and $C_\beta H_2$ (Figure 6A) of a His and the $C_\alpha H$ (Figure 6B) of another residue, in a fashion very similar to that observed in PH*IX* and DMDH*IX* complexes.[24,35] The molecular model and C-terminal deletions have shown[24] that these contacts involve His207 and the $C_\alpha H$ of Arg208.

The reference spectrum of the *Nm*HO−(6P→M)PH*IX*-N_3 complex exhibits somewhat broader peaks than the other complexes but still allows the necessary assignments (Figure S3 of the Supporting Information). The weak, resolved inter-methyl cross-peak that identifies M_1/M_8 and their cross-peaks to the Cys113 $C_\alpha H$ demonstrate that the orientation of the substrate is rotated 180° about the α,γ-meso position relative to native PH*IX* in the crystal (as shown in Figure 3B). Strongly upfield shifted vinyl H_βs exhibit weak cross-peaks to the remaining low-field methyl and to the vinyl H_α, which in turn exhibits a cross-peak to a partially resolved methyl, identifying M_5, M_3, and the 4-vinyl in the *trans* orientation (as shown in Figure 3B). A cross-peak from M_1 to a vinyl H_α shows that the 2-vinyl is similarly in the *trans* orientation (as depicted in Figure 3B). M_5 in the 180°-rotated orientation exhibits cross-peaks to a His $C_\beta H_2$ and the $C_\alpha H$ of another residue that dictates their origin as His207 and Arg208.

The NOESY spectrum of the *Nm*HO−(7P→M)DMDH*IX*-N_3 complex (Figure S4 of the Supporting Information) reveals three pairs of strongly coupled methyls with weak coupling between the pairs, and another weak coupling to a seventh

methyl that uniquely identify M_1−M_5, M_7, and M_8. The contacts from M_5 to C_βHs locate the 6-propionate. The cross-peaks from M_1/M_8 to Phe123 and those from M_5/M_4 to Cys113 uniquely determine the orientation in which the lone propionate occupies the same position as the 6-propionate in the crystal structure (Figure 3E). M_8/M_1 exhibits NOESY cross-peaks to both the C_βHs and C_δH of a His and the C_αH of another residue that identify His207 and Arg208. It is noted that contacts from M_8 to both the backbone and ring of His207 exist; this latter contact was much weaker or undetected in the complexes with the native PH*IX* (or DMDH*IX*) possessing the normal propionates at both positions 6 and 7.

The NOESY spectrum of the *Nm*HO−(7P→M:8M→P)DMDH*IX*-N_3 complex depicts two pairs of strongly coupled methyls that collectively identify the M_1/M_2 and M_3/M_4 pairs. A weak cross-peak between the pairs, as well as a weak NOE from one of the pairs to a low-field methyl, identifies M_1−M_5; the contacts from M_5 to a C_αH locate the 6-propionate (Figure S5 of the Supporting Information). A less strongly low-field shifted methyl exhibits cross-peaks to a low-field shifted C_αH and C_βHs of a propionate identifying the remaining M_7 and 8-propionate; $H_{8\alpha}$ exhibits a weak cross-peak to M_1. Contacts of M_1/M_8 with Phe123 and M_4/M_5 with Cys113 establish the orientation with one propionate occupying the crystallographic 6-propionate position and the other the crystallographic 8-positions (as depicted in Figure 3F). The contact from $H_{8\alpha}$ to a C_αH of one residue and contacts from $M_1/H_{8\alpha}$ to the C_βHs of an apparent His represent the interaction of His207 and Arg208 with the active site. It was not possible to locate the His207 C_δH, but cross-peaks from M_1 and $H_{8\alpha}$ to C_βHs not predicted by the crystal structure indicate their origin as His207.

The NOESY spectrum of the *Nm*HO−PH*XIII*-N_3 complex (not shown) identifies all the substrate signals with the NOESY cross-peak from the 1-vinyl $H_{1\beta}$ to M_8 and Phe123 and the cross-peak from $H_{1\alpha}$ to M_2, indicating that the vinyl group is in a *trans* position (as depicted in Figure 3C). The 4-vinyl group exhibits the same cross-peaks as in PH*IX* and hence retains the conventional *cis* orientation. The cross-peaks from $M_8/H_{1\beta}$ to a $C_\beta H_2$ group and the cross-peak from M_8 to a C_αH locate His207 and Arg208. All chemical shift data are provided in Tables S1 and S3 of the Supporting Information.

Loss of Substrate−Residue Contacts upon NmHO "Aging". Over a period of a few days at 25 °C, the resolved resonances of the complexes of WT *Nm*HO with (7P→M)PH*IX*, (7P→M)DMDH*IX*, and (7P→M:8M→P)DMDH*IX* disappear and are replaced in the conversion to an "aged", or homogeneously degraded, derivative (*Nm*HO^X). The reference spectra for the three aged derivatives are illustrated as Figure 4B′ and as spectra B′ and C′ of Figure 5, respectively. Concomitant with the generation of *Nm*HO^X is the appearance of two very narrow resonances in the aromatic spectral window. A similar conversion of *Nm*HO to *Nm*HO^X has been characterized in detail for both PH*IX* and DMDH*IX* complexes and the product shown[21,22] to be the result of cleavage of the Arg208His209 dipeptide. In contrast, the complexes of WT *Nm*HO with (5P→M)PH*IX* and PH*XIII* exhibit only minor (<10%) amounts of aging over the same period of time, dictating that the terminal cleavage rate must be significantly (factor of >10) slower than that of either the other propionate modified or native PH*IX* and DMDH*IX* substrates. Unfortunately, the very sparingly available complexes of the propionate-modified substrates were heterogeneously decomposed upon completion of 2D NMR, precluding meaningful mass spectrometric studies for characterizing the initially cleaved peptide.

The NOESY spectrum of the *Nm*HO^X−(7P→M)PH*IX*-N_3 complex provides the same assignment as that of the WT *Nm*HO complex (not shown). The most prominent difference is that the contacts from M_1/M_8 to His207 and Arg208 are lost (see Figure 6A′). Similar NOESY data for the complexes of *Nm*HO^X with (7P→M)DMDH*IX* and (7P→M:8M→P)-DMDH*IX* (Figures S6 and S7 of the Supporting Information, respectively), in each case, exhibit not only a largely conserved active site structure but also the loss of the contacts from M_1/M_8 and $M_1/H_{1\alpha}$ to His207 and Arg208. The loss of these contacts is consistent with cleavage of the C-terminus. The substrate chemical shifts are perturbed upon aging in a manner similar to that observed[21,23] for PH*IX* and DMDH*IX*. Active site residue chemical shifts are only inconsequentially perturbed by aging. Both substrate (Tables S1 and S2 of the Supporting Information) and active site residue (Tables S3 and S4 of the Supporting Information) chemical shifts for the *Nm*HO^X complexes are provided in the Supporting Information.

Effect of C-Terminal Cleavage on the Substrate Propionate Carboxylates. The conversion of the native *Nm*HO−PH*IX*−H_2O complex to yield the *Nm*HO^X−PH*IX*−H_2O complex by the loss of the Arg208His209 peptide is relatively rapid (half-life of 24 h) and is readily followed[22] by ^{1}H NMR via the relative intensities of the resolved M_8 peaks. Figure 7A provides the ^{13}C NMR spectrum in the carboxylate

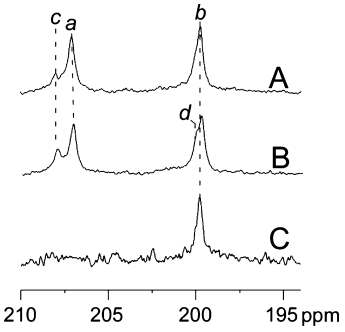

Figure 7. Portion of the 151 MHz ^{13}C NMR reference spectrum for the carboxylate chemical shift window for (A) ∼90% WT *Nm*HO−(6,7-$^{13}CO_2^-$)$_2$PH*IX*−H_2O complex and ∼10% C-terminally cleaved *Nm*HO^X−(6,7-$^{13}CO_2^-$)$_2$PH*IX*−H_2O complex, (B) ∼70% WT *Nm*HO−(6,7-$^{13}CO_2^-$)$_2$PH*IX*−H_2O complex and ∼30% C-terminally cleaved *Nm*HO^X−(6,7-$^{13}CO_2^-$)$_2$PH*IX*−H_2O complex, and (C) ∼75% WT *Nm*HO−(6-$^{13}CO_2^-$)PH*IX*−H_2O complex and ∼25% C-terminally cleaved *Nm*HO^X−(6-$^{13}CO_2^-$)PH*IX*−H_2O complex. Peaks *a* and *b* are assigned to the 7- and 6-propionate carboxylates, respectively, in the WT *Nm*HO complex, and peaks *c* and *d* to the 6- and 7-carboxylates, respectively, in the C-terminally cleaved *Nm*HO^X complex.

spectral window for the *Nm*HO−(6,7-$^{13}CO_2^-$)$_2$PH*IX*−H_2O complex (∼90% *Nm*HO and ∼10% *Nm*HO^X), which reveals two well-spaced signals, labeled *a* and *b*, uniquely attributable to the two labeled carboxylates. The spectrum of this complex upon ∼25% degradation to *Nm*HO^X is shown in Figure 7B and identifies the degraded species with peaks labeled *c* and *d*; clearly, the chemical shift for one propionate is conserved upon C-terminal cleavage, while the other is significantly perturbed. The ^{13}C NMR spectrum of a partially degraded, singly labeled complex, *Nm*HO−(6-$^{13}CO_2^-$)PH*IX*−H_2O (∼75% *Nm*HO,

dx.doi.org/10.1021/bi3007803 | *Biochemistry* 2012, 51, 7054−7063

~25% *Nm*HO^X), is shown in Figure 7C and confirms that the propionate sensitive to C-terminal cleavage is clearly that at the crystallographic 7-position.

DISCUSSION

Structure of the Active Site. Both UV−visible and ^{1}H NMR spectroscopy clearly show that each of the propionate-modified substrates is quantitatively incorporated into the active site of *Nm*HO; standard in vitro assays[22] show that the complexes retain full activity. The ^{1}H NMR data establish that the substrates seat overwhelmingly in a single orientation that in each case dictates that the only propionate protein salt bridge crucial to substrate binding to *Nm*HO is that between Lys16 and the 6-propionate position in the crystal structure.[9,11] The strong conservation of active site structure, in spite of the drastic propionate deletion and/or rearrangement, is confirmed by not only the conserved pattern of NOESY cross-peaks but also the conservation of the pattern of hyperfine shifts. On one hand, nonligated active site residues exhibit only dipolar shifts[36,45] that sensitively reflect the anisotropy and/or orientation of the paramagnetic susceptibility tensor, χ, and the position of the residue. Even small changes in the orientation of χ can result in large changes in the dipolar shift pattern.[23,46] The dipolar shifts for crystallographically detected active site residues are highly conserved among the variable substrates and upon C-terminal cleavage (Tables S3 and S4 of the Supporting Information), dictating that both the orientation of χ and the residue geometries are conserved among the complexes.

On the other hand, ligated His23 and substrate hyperfine shifts are dominated by the contact interaction[36,45] (and, to a lesser degree, by 2,4-substituents).[47] The data in Table 1 show that the pattern of the His23 C_βHs, and hence the orientation of the His imidazole relative to the protein matrix, is conserved for the various substituents. Substrate methyls very sensitively reflect the in-plane rotational orientation of the substrate relative to the axial histidine imidazole plane[36,48] and, by inference, the protein matrix. Thus, the pattern of the M_1, M_3, M_5, and M_8 shifts is inconsequentially differentiated within the pair of complexes of PH*IX* and (7P→M)PH*IX*-N_3 (see Table 1); the same highly conserved M_1−M_5 shift pattern is observed within the three complexes of DMDH*IX*, (7P→M)DMDH*IX*-N_3, and (7P→M:8M→P)DMDH*IX*. For the (6P→M)PH*IX* complex with the "reversed" orientation (Figure 3B), the pattern of methyl shifts is conserved relative to that for the equilibrium ~20% populated reversed orientation[27] of native PH*IX* (data in column 2 of Table 1). This dictates that the in-plane orientation of the substrate is inconsequentially affected by either deletion or rearrangement of one of the propionates. Lastly, the low-field bias for H-bond signals for Gln49 and His53, which are linked to the axial ligand via the catalytic water molecules,[9,11] is strictly conserved.

Structure of the C-Terminus and Its Cleavage. Each of the *Nm*HO complexes of these propionate-modified substrates exhibits contacts to residues at the crystallographically exposed 1- and 8-positions [i.e., the positions of the PH*IX* 1CH_3 and CH_3 groups in the crystal structure (Figure 1B)] that are not described in the crystal structure in which the C-terminal His207Arg208His209 fragment is undetected.[9,11] This absence in the crystal was attributed to structural disorder, but possible loss of the C-terminus by an unusual degradation clearly established in solution by ^{1}H NMR and mass spectrometry[22] has not yet been ruled out. In any case, these contacts have been assigned to His207 and Arg208 and were confirmed by C-terminal deletion.[22] A molecular model[24] based on limited energy minimization using NOESY constraints and a series of three salt bridges and one H-bond involving the three C-terminal residues, the side chain of Lys126, the carboxylate of Asp27, and the propionate at the crystallographic 7-position, is reproduced in Figure 2. The observation of very similar interactions of His207 and Arg208 with the active site with each of the modified substrates indicates that the architecture of the interaction of the C-terminus with the active site is qualitatively retained upon loss of the 7-propionate−Arg208 salt bridge.

The relatively modest effect on the C-terminal structure upon deletion of the 7-propionate could be attributed to the failure of the 7-propionate to interact with the C-terminus, as described by our model.[22,24] However, the ^{13}C chemical shift for the PH*IX* propionate carboxylates (Figure 7) is strongly perturbed for the 7-propionate, but not for the 6-propionate, upon C-terminal cleavage, confirming that the 7-propionate does interact with the C-terminus in the native complex. The loss of the 7-propionate salt bridge may weaken, but not significantly rupture, the interaction of the C-terminus with the active site. This confirms the relatively robust nature of this interaction of the C-terminus with the active site.[24] Qualitative changes upon deletion of the 7-propionate include slightly altered hyperfine shifts for His207 in spite of conserved χ, and more intense NOESY cross-peaks between 8CH_3 and the His207 C_δH than in complexes with the native propionates. Inasmuch as the C-terminal interaction with the active site in 7-propionate-deleted substrates is not biologically relevant, no attempt was made to model this interaction.

It is not clear whether the propionate at the crystallographic 8-position in the *Nm*HO−(7P→M:8M→P)DMDH*IX*-N_3 complex interacts with the terminus of Arg208. The molecular model suggests that the carboxylate of the 8-propionate could orient to form the salt bridge. The fact that the C-terminal cleavage leads to significant chemical shift changes for the 8-propionate C_βH chemical shifts (−1.50 and −0.80 ppm in WT *Nm*HO to −0.80 and −0.49 in *Nm*HO^X) suggests that a salt bridge between the 8-propionate and Arg208 side chain may exist in this complex.

NMR studies[22,24] with variably 2-,4-disubstituted substrates had shown that the rate of C-terminal cleavage correlates with the proximity of His207 to the substrate, with the rate of cleavage significantly enhanced upon replacement of the bulky vinyls with methyls or hydrogens. Both (6P→M)PH*IX* and PH*XIII* have the vinyl at the crystallographic 1 position oriented *trans* [H_βs close to position 8 (see Figure 3B,C)], which will sterically interfere with His207 approaching the substrate. The retarded rates of cleavage for these two modified substrates are consistent with its model.

Comparison to Other HOs and Functional Implications. Clearly, *Nm*HO requires but a single propionate salt bridge to the protein matrix to effectively bind substrate, in contrast to mammalian HO.[15,16] Moreover, protohemin-I [the analogue to (7P→M:8M→P)PH*IX*, but with 2,4-vinyls] fails to yield an active hHO complex.[15] In contrast, the (7P→M:8M→P)PH*IX* complex (Figure 3F) retains full activity in *Nm*HO. The fact that deletion of one propionate abolishes substrate binding for hHO but not *Nm*HO dictates that other substrate−enzyme interactions must be stronger in the *Nm*HO complex than in the hHO complex. Because one salt bridge between the propionate at position 6 (Figure 1) and the side chain terminus of a Lys (Lys16 for *Nm*HO and Lys18 for hHO) is conserved,

it is reasonable to attribute the stronger interactions in *Nm*HO to van der Waals contacts primarily with pyrroles A and B. Stronger van der Waals interactions have been implied in the much more compact active site in crystals.[2,9,11] A similar conclusion has been reached on the basis of the much stronger orientational preference of substrates about the α,γ-meso axis[27] when compared to other HOs.[20,28−30] Hence, the stronger substrate−enzyme van der Waals interactions in *Nm*HO−substrate complexes can be viewed as a mechanism for "liberating" one of the two propionates for a functional role unnecessary in other HOs, namely the ordering of the C-terminus to interact with the active site.

The solution NMR-detected C-terminal interaction with the active site can be expected to have functional implications for two distinct processes that most likely occur at the exposed substrate edge that, in *Nm*HO, is "shielded" by the interaction of the C-terminus with the active site.[24] On one hand, HO−biliverdin complexes dissociate too slowly to sustain effective biological catalysis.[25] For mammalian systems, the product biliverdin is not released until a transient 1:1 complex is formed with BVR with contact at the exposed substrate edge.[26] The BVR acts as a cooperative facilitator that significantly accelerates the rate of biliverdin release and at the same time precludes the presence of significant concentrations of the toxic biliverdin. While bilirubin may not be toxic for bacteria, there is still the need for the transient binding of an allosteric effector (the BVR analogue) to accelerate biliverdin release. On the other hand, while cytochrome-P450 reductase and NADPH or ascorbate react with mammalian systems directly to yield iron-free biliverdin,[3] the same reactions with *Nm*HO complexes proceed only to the iron(III)−biliverdin complex where the iron can be extracted by only a powerful iron chelator.[2,49] The final reduction step for *Nm*HO complexes must rely on the specific *Nm*HO electron donor. It is possible that once the iron biliverdin complex of *Nm*HO is formed, the native electron donor protein may serve as both a source of the key electron for the iron and an allosteric effector to labilize the resulting iron-free biliverdin. Unfortunately, neither the BVR analogue nor the electron donor in pathogenic bacteria is known.[2] A more detailed understanding of the fate of biliverdin in *N. meningitidis* would be necessary to provide fruitful insight into the unique C-terminal structural role of *Nm*HO.

CONCLUSIONS

*Nm*HO binds substrates possessing a single propionate to form active complexes by either deleting or rearranging the position of one of the propionates of the substrate. This is in strong contrast with the situation in hHO where neither propionate deletion nor rearrangement affords an active complex. The unique salt bridge for *Nm*HO is between the propionate at the crystallographic 6-position and the terminus of Lys16. The second substrate propionate at the normal crystallographic 7-position (and possibly at the unprecedented 8-position) forms a salt bridge to the (crystallographically undetected) side chain of Arg208 as a portion of the stabilization of the interactions of the C-terminus with the active site. The solvent-exposed side of the substrate consisting of the crystallographic 1- and 8-positions interacts with the C-terminus in a qualitatively conserved manner upon elimination of the 7-propionate, as described by an earlier molecular model,[24] although altered hyperfine shifts suggest some minor rearrangement in the architecture of the C-terminus. Spontaneous C-terminal cleavage abolishes the characteristic contacts between the C-terminus and active site, with the exception of substrates oriented with the vinyl group at the crystallographic 1-position, which interferes with the interaction of the C-terminus with the active site. The effective binding of a substrate with a single propionate by *Nm*HO, instead of the two required from mammalian HOs, is attributed to a larger contribution to the substrate binding from peripheral van der Waals interactions, as supported by more compact structure,[2,9,11] fewer vacancies, and the much stronger orientational preference about the α,γ-meso axis.[27] These structural differences are proposed to have evolved, in part, to liberate one propionate for stabilizing interactions of the active site with the C-terminus, which, in turn, is proposed to function in product release.

ASSOCIATED CONTENT

Supporting Information

Seven figures (UV−visible spectra, enzyme assays, and five 2D NOESY spectra) and four tables (substrate and active site residue chemical shifts for PH*IX* and DMDH*IX* derivatives). This material is available free of charge via the Internet at http://pubs.acs.org.

AUTHOR INFORMATION

Corresponding Author

*E-mail: lamar@chem.ucdavis.edu. Phone: (530) 752-0958. Fax: (530) 752-8995.

Funding

This research was supported by grants from the National Institutes of Health [GM62830 (G.N.L.) and CA132861 (K.M.S.)]. The purchase of the NMR instrumentation was supported by grants from the National Institutes of Health (RR1973) and the National Science Foundation (DBIO722538).

Notes

The authors declare no competing financial interest.

ABBREVIATIONS

BVR, biliverdin reductase; DSS, 2,2-dimethyl-2-silapentane-5-sulfonate; HO, heme oxygenase; hHO, human heme oxygenase-1; *Nm*HO, *N. meningitidis* heme oxygenase; *Cd*HO, *C. diphtheriae* heme oxygenase; *Pa*HO, *P. aeruginosa* heme oxygenase; NOESY, two-dimensional nuclear Overhauser effect spectroscopy; TOCSY, two-dimensional total correlation spectroscopy; ROESY, rotating-frame two-dimensional Overhauser spectroscopy; PH*IX*, protohemin-IX; PH*XIII*, protohemin-XIII; DMDH*IX*, 2,4-dimethyldeuterohemin-IX; (6P→M)PH*IX*, 6-depropionate-, 6-methyl-protohemin-IX; (7P→M)PH*IX*, 7-depropionate-, 7-methyl-protohemin-IX; (7P→M)DMDH*IX*, 7-depropionate-, 7-methyl-2,4-dimethyldeuterohemin-IX; (7P→M:8M→P)DMDH*IX*, 7-depropionate-7-methyl-, 8-demethyl-8-propionate-2,4-dimethyldeuterohemin-IX.

REFERENCES

(1) Tenhunen, R., Marver, H. S., and Schmid, R. (1969) Microsomal heme oxygenase. Characterization of the enzyme. *J. Biol. Chem. 244*, 6388−6394.

(2) Wilks, A. (2002) Heme Oxygenase: Evolution, Structure, and Mechanism. *Antioxid. Redox Signaling 4*, 603−614.

(3) Ortiz de Montellano, P. R., and Auclair, K. (2003) Heme Oxygenase Structure and Mechanism. In *The Porphryin Handbook* (Kadish, K. M., Smith, K. M., and Guilard, R., Eds.) pp 175−202, Elsevier Science, San Diego.

(4) Frankenberg-Dinkel, N. (2004) Bacterial Heme Oxygenases. *Antoxid. Redox Signaling 6*, 825−834.
(5) Rivera, M., and Zeng, Y. (2005) Heme oxygenase, steering dioxygen activation toward heme hydroxylation. *J. Inorg. Biochem. 99*, 337−354.
(6) Unno, M., Matsui, T., and Ikeda-Saito, M. (2007) Structure and catalytic mechanism of heme oxygenase. *Nat. Prod. Rep. 24*, 553−570.
(7) Beale, S. I. (1994) Biosynthesis of open-chain tetrapyrroles in plants, algae, and cyanobacteria. *Ciba Found. Symp. 180*, 156−168.
(8) Schuller, D. J., Wilks, A., Ortiz de Montellano, P. R., and Poulos, T. L. (1999) Crystal structure of human heme oxygenase-1. *Nat. Struct. Biol. 6*, 860−867.
(9) Schuller, D. J., Zhu, W., Stojiljkovic, I., Wilks, A., and Poulos, T. L. (2001) Crystal structure of heme oxygenase from the Gram-negative pathogen *Neisseria meningitidis* and a comparison with mammalian heme oxygeanse-1. *Biochemistry 40*, 11552−11558.
(10) Sugishima, M., Sakamoto, H., Higashimoto, Y., Omata, Y., Hayashi, S., Noguchi, M., and Fukuyama, K. (2002) Crystal structure of rat heme oxygenase-1 in complex with heme bound to azide: Implication for regiospecific hydroxylation of heme at the *α-meso* carbon. *J. Biol. Chem. 277*, 45086−45090.
(11) Friedman, J. M., Lad, L., Deshmukh, R., Li, H. Y., Wilks, A., and Poulos, T. L. (2003) Crystal structures of the NO- and CO-bound heme oxygenase from *Neisseriae meningitidis*: Implications for O_2 activation. *J. Biol. Chem. 278*, 34654−34659.
(12) Unno, M., Matsui, T., Chu, G. C., Coutoure, M., Yoshida, T., Rousseau, D. L., Olson, J. S., and Ikeda-Saito, M. (2004) Crystal Structure of the Dioxygen-bound Heme Oxygenase from *Corynebacterium diphtheriae*. *J. Biol. Chem. 279*, 21055−21061.
(13) Friedman, J., Lad, L., Li, H., Wilks, A., and Poulos, T. L. (2004) Structural Basis for Novel *δ*-Regioselective Heme Oxygenation in the Opportunistic Pathogen *Pseudomonas aeruginosa*. *Biochemistry 43*, 5239−5245.
(14) Wang, J., Evans, J. P., Ogura, H., La Mar, G. N., and Ortiz de Montellano, P. R. (2006) Alteration of the Regiospecificity of Human Heme Oxygenase-1 by Unseating of the Heme but not Disruption of the Distal Hydrogen Bonding Network. *Biochemistry 45*, 61−73.
(15) Frydman, R. B., Tomaro, M. L., Buldain, G., Awruch, J., Diaz, L., and Frydman, B. (1981) Specificity of heme oxygenase: A study with synthetic hemins. *Biochemistry 20*, 5177−5182.
(16) Tomaro, M. L., Frydman, S. B., Frydman, B., Pandey, R. K., and Smith, K. M. (1984) The Oxidation of Hemins by Microsomal Heme Oxygenase: Structural Requirements for the Retention of Substrate Activity. *Biochim. Biophys. Acta 791*, 342−349.
(17) Matsui, T., Furukawa, M., Unno, M., Tomita, T., and Ikeda-Saito, M. (2005) Roles of Distal Asp in Heme Oxygenase from *Corynebacterium diphtheriae*, HmuO. *J. Biol. Chem. 280*, 2981−2989.
(18) Zeng, Y., Deshmukh, R., Caignan, G. A., Bunce, R. A., Rivera, M., and Wilks, A. (2004) Mixed Regioselectivity in the Arg-177 Mutants of *Corynebacterium diphtheriae* Heme Oxygenase as a Consequence of in-Plane Heme Disorder. *Biochemistry 43*, 5222−5238.
(19) Koenigs Lightning, L., Huang, H.-W., Moënne-Loccoz, P., Loehr, T. M., Schuller, D. J., Poulos, T. L., and Ortiz de Montellano, P. R. (2001) Disruption of an active site hydrogen bond converts human heme oxygenase-1 into a peroxidase. *J. Biol. Chem. 276*, 10612−10619.
(20) Caignan, G. A., Deshmukh, R., Wilks, A., Zeng, Y., Huang, H.-w., Moenne-Loccoz, P., Bunce, R. A., Eastman, M. A., and Rivera, M. (2002) Oxidation of heme to *β*- and *δ*-biliverdin by *Pseudomonas aeruginosa* Heme Oxygenase as a Consequence of an Unusual Seating of the Heme. *J. Am. Chem. Soc. 124*, 14879−14892.
(21) Liu, Y., Zhang, X., Yoshida, T., and La Mar, G. N. (2004) ^{1}H NMR characterization of the solution active site structure of substrate-bound, cyanide-inhibited heme oxygenase from *Neisseria meningitidis*; comparison to crystal structures. *Biochemistry 43*, 10112−10126.
(22) Liu, Y., Ma, L.-H., Satterlee, J. D., Zhang, X., Yoshida, T., and La Mar, G. N. (2006) Characterization of the spontaneous "aging" of the heme oxygenase from the pathological bacterium *Neisseria meningitidis* via cleavage of the C-terminus in contact with the substrate; implications for functional studies and the crystal structure. *Biochemistry 45*, 3875−3886.
(23) Liu, Y., Ma, L.-H., Zhang, X., Yoshida, T., Satterlee, J. D., and La Mar, G. N. (2006) ^{1}H NMR study of the influence of hemin vinyl-methyl substitution on the interaction between the C-terminus and substrate and the "aging" of the heme oxygenase from *N. meningitidis*. Induction of active site structural heterogeneity by a two-fold symmetric hemin. *Biochemistry 45*, 13875−13888.
(24) Peng, D., Ma, L.-H., Ogura, H., Yang, E.-C., Zhang, X., Yoshida, T., and La Mar, G. N. (2010) ^{1}H NMR Study of the Influence of Mutation on the Interaction of the C-Terminus with the Active Site in Heme Oxygenase from *Neisseria meningitidis*: Implications for Product Release. *Biochemistry 49*, 5832−5840.
(25) Liu, Y., and Ortiz de Montellano, P. R. (2000) Reaction Intermediates and Single Turnover Rate Constants for the Oxidation of Heme by Human Heme Oxygenase-1. *J. Biol. Chem. 275*, 5297−5307.
(26) Wang, J., and Ortiz de Montellano, P. R. (2003) The Binding Sites on Human Heme Oxygenase-1 for Cytochrome P450 Reductase and Biliverdin Reductase. *J. Biol. Chem. 278*, 20069−20076.
(27) Peng, D., Satterlee, J. D., Ma, L.-H., Dallas, J. L., Smith, K. M., Zhang, X., Sato, M., and La Mar, G. N. (2011) Influence of Substrate Modification and C-Terminal Truncation on the Active Site Structure of Substrate-Bound Heme Oxygenase from *Neisseriae meningitidis*. A ^{1}H NMR Study. *Biochemistry 50*, 8823−8833.
(28) Hernández, G., Wilks, A., Paolesse, R., Smith, K. M., Ortiz de Montellano, P. R., and La Mar, G. N. (1994) Proton NMR Investigation of Substrate-bound Heme Oxygenase: Evidence for Electronic and Steric Contributions to Stereoselective Heme Cleavage. *Biochemistry 33*, 6631−6641.
(29) Gorst, C. M., Wilks, A., Yeh, D. C., Ortiz de Montellano, P. R., and La Mar, G. N. (1998) Solution ^{1}H NMR investigation of the molecular and electronic structure of the active site of substrate-bound human heme oxygenase: The nature of the distal hydrogen bond donor to bound ligands. *J. Am. Chem. Soc. 120*, 8875−8884.
(30) Li, Y., Syvitski, R. T., Chu, G. C., Ikeda-Saito, M., and La Mar, G. N. (2003) Solution ^{1}H NMR investigation of the active site molecular and electronic structures of the substrate-bound, cyanide-inhibited bacterial heme oxygenase from *C. diphtheriae*. *J. Biol. Chem. 279*, 6651−6663.
(31) Smith, K. M., Fujinari, E. M., Langry, K. C., Parish, D. W., and Tabba, H. D. (1983) Manipulation of Vinyl Groups in Protoporphyrin-IX: Introduction of Deuterium and Carbon-13 Labels for Spectroscopic Studies. *J. Am. Chem. Soc. 105*, 6638−6646.
(32) Smith, K. M., and Craig, G. W. (1983) Porphyrin Synthesis Through Tripyrrins: An Alternate Approach. *J. Org. Chem. 48*, 4302−4306.
(33) Ogura, H., Evans, J. P., Peng, D., Satterlee, J. D., Ortiz de Montellano, P. R., and La Mar, G. N. (2009) The Orbital Ground State of the Azide-Substrate Complex of Human Heme Oxygenase Is an Indicator of Distal H-Bonding: Implications for the Enzyme Mechanism. *Biochemistry 48*, 3127−3132.
(34) Zeng, Y., Caignan, G. A., Bunce, R. A., Rodriguez, J. C., Wilks, A., and Rivera, M. (2005) Azide-inhibited Bacterial Heme Oxygenases Exhibit an S=3/1 $(d_{xz},d_{yz})^3(d_{xy})^1(d_z{}^2)^1$ Spin State: Mechanistic Implications for Heme Oxidation. *J. Am. Chem. Soc. 127*, 9794−9807.
(35) Ma, L.-H., Liu, Y., Zhang, X., Yoshida, T., and La Mar, G. N. (2009) ^{1}H NMR study of the effect of variable ligand on heme oxygenase electronic and molecular structure. *J. Inorg. Biochem. 103*, 10−19.
(36) La Mar, G. N., Satterlee, J. D., and de Ropp, J. S. (2000) NMR of Hemoproteins. In *The Porphyrin Handbook* (Kadish, K. M., Smith, K. M., and Guilard, R., Eds.) pp 185−298, Academic Press, San Diego.
(37) Smith, K. M., Pandey, R. K., and Tabba, H. D. (1986) Syntheses of Derivatives of Protoporphyrin-IX Regioselectively Enriched in the Propionic Side Chains with Carbon-13. *J. Chem. Res., Synop.,* 402−403.
(38) Hauksson, J. B., La Mar, G. N., Pandey, R. K., Rezzano, I. N., and Smith, K. M. (1990) NMR Study of Heme Pocket Polarity/

Hydrophobicity of Myoglobin Using Polypropionate-Substituted Hemins. *J. Am. Chem. Soc. 112*, 8315−8323.
(39) Kikuchi, A., Park, S. Y., Miyatake, H., Sun, D., Sato, M., Yoshida, T., and Shiro, Y. (2001) Crystal structure of rat biliverdin reductase. *Nat. Struct. Biol. 8*, 221−225.
(40) Jeener, J., Meier, B. H., Bachmann, P., and Ernst, R. R. (1979) Investigation of Exchange Processes by Two Dimensional NMR Spectroscopy. *J. Chem. Phys. 71*, 4546−4553.
(41) Griesinger, C., Otting, G., Wüthrich, K., and Ernst, R. R. (1988) Clean TOCSY for ^{1}H Spin System Identification in Macromolecules. *J. Am. Chem. Soc. 110*, 7870−7872.
(42) Wishart, D. S., Bigam, C. G., Holm, A., Hodges, R. S., and Sykes, B. D. (1995) ^{1}H, ^{13}C and ^{15}N Random Coil Chemical Shifts of the Common Amino Acids: I. Investigation of Nearest Neighbor Effects. *J. Biomol. NMR 5*, 67−81.
(43) Zhu, W., Willks, A., and Stojiljkovic, I. (2000) Degradation of heme in Gram-negative bacteria: The product of the hemO gene of *Neisseriae* is a heme oxygenase. *J. Bacteriol. 182*, 6783−6790.
(44) Wüthrich, K. (1986) *NMR of Proteins and Nucleic Acids*, Wiley & Sons, New York.
(45) Bertini, I., and Luchinat, C. (1996) NMR of Paramagnetic Substances. *Coord. Chem. Rev. 150*, 1−296.
(46) Zhu, W., Li, Y., Wang, J., Ortiz de Montellano, P. R., and La Mar, G. N. (2006) Solution NMR study of environmental effects on substrate seating in human heme oxygenase; influence of polypeptide truncation, substrate modification and axial ligand. *J. Inorg. Biochem. 100*, 97−107.
(47) Kolczak, U., Hauksson, J. B., Davis, N. L., Pande, U., de Ropp, J. S., Langry, K. C., Smith, K. M., and La Mar, G. N. (1999) ^{1}H NMR investigation of the role of intrinsic heme versus protein-induced rhombic perturbations on the electronic structure of low-spin ferrihemoproteins: Effect of heme substituents on heme orientation in myoglobin. *J. Am. Chem. Soc. 121*, 835−843.
(48) Shokhirev, N. V., and Walker, F. A. (1998) The Effect of Axial Ligand Plane Orientation on the Contact and Pseudocontact Shifts of Low-spin Ferriheme Proteins. *J. Biol. Inorg. Chem. 3*, 581−594.
(49) Zhu, W., Wilks, A., and Stojiljkovic, I. (2000) Degradation of Heme in Gram-Negative Bacteria: The Product of the hemO Gene of *Neisseriae* Is a Heme Oxygenase. *J. Bacteriol. 182*, 6783−6790.